

PAPER

Green-solvent-processed lead-free perovskite solar cells

View the [article online](#) for updates and enhancements.

You may also like

- [Improving the Performance of Invert Perovskite Solar Cell Devices By a Multifunctional Ammonium Salt](#)
Yifang Qi and Qilin Dai
- [Interface Engineering for Highly Efficient Perovskite Photovoltaics](#)
Nga Phung, Andrea Bracesco and Mariadriana Creatore
- [Structure-Controlled Perovskite Thin Layer Formation on Au Single-Crystal Substrate via Self-Assembled Monolayer of 4-Aminothiophenol](#)
Mami Takahari and Toshihiro Kondo

Green-solvent-processed lead-free perovskite solar cells

Linfeng He^{1,2}, Xin Zhang², Xinyao Chen¹, Jin Cheng¹, Zhenjun Li³ and Junming Li^{1,2,*} 

¹ Beijing Key Laboratory for Sensor, School of Applied Science, Beijing Information Science and Technology University, Beijing 100101, People's Republic of China

² Key Laboratory of Modern Measurement & Control Technology, Ministry of Education, Beijing Information Science and Technology University, Beijing 100192, People's Republic of China

³ CAS Key Laboratory of Standardization and Measurement for Nanotechnology, CAS Key Laboratory of Nanophotonic Materials and Devices (Preparatory), National Center for Nanoscience and Technology, Beijing 100190, People's Republic of China

E-mail: li@bistu.edu.cn

Received 10 May 2024, revised 21 July 2024

Accepted for publication 24 July 2024

Published 1 August 2024



Abstract

Tin-based perovskite has been considered as one of the most potential candidates for lead-based perovskite. The solution proceed method was widely utilized in fabricating tin perovskite solar cells. So far, all fabrication processes for tin perovskite solar cells involved toxic organic solvents, which is contrary to the development of environmentally friendly perovskite solar cells. In this study, we report for the first time, by using a mixed green solvent N-diethyl formamide and green 1,3-dimethyl-3,4,5,6-Tetrahydro-2 (1H)-pyrimidinone as precursor solvent, and a green solvent dibutyl ether as antisolvent, a high-quality $\text{FA}_{0.75}\text{MA}_{0.25}\text{SnI}_3$ film was achieved. The optical band gap of the prepared perovskite layer was 1.36 eV, which was close to the ideal band gap. The green-solution-proceed perovskite films showed reduced defect density. As a consequence, the champion green-solution-proceed photovoltaic device achieved a power conversion efficiency of 4.4%. Moreover, it still maintains 80% of the initial efficiency after 600 h of storage in a nitrogen atmosphere. This work would promote the perovskite solar cells from a 'new' technique to a 'new and green' technique.

Supplementary material for this article is available [online](#)

Keywords: green solution, solution proceed, green antisolvent, tin-based perovskite, interface

1. Introduction

As a competitive candidate in the emerging-generation photovoltaic technology, perovskite solar cells (PSCs) have received widespread attention because of their excellent photoelectric properties, such as light-weight, fast-fabrication process, and feasible low cost, *etc* [1–3]. Today, all high-efficiency PSCs contain toxic lead ions, which raises environmental and human health concerns [4, 5]. Tin-based perovskite has been considered as a mostly likely substitute for its lead counterpart, attributed to its excellent optoelectrical properties such as high

carrier mobility (up to $143 \text{ cm}^{-2}\text{V}^{-1}\text{S}^{-1}$), and low exciton binding energy (18 meV), *etc* [6–8]. Meanwhile, tin-based perovskites (ASnI_3 , A = Cs, FA, MA, *etc*) have been reported to have a band gap in the range of 1.2–1.4 eV [9], which is very close to the optimal band gap at the Schottky limit (1.34 eV) [10], and this ideal band gap is considered to be the biggest driving force for the development of tin-based lead-free perovskite materials. Nowadays, the certified PCE of tin-based perovskite photovoltaic devices has reached up to 14.6% [11]. However, the performance was still lower than its lead counterpart, mainly due to two reasons: firstly, the Sn^{2+} is easily oxidized to Sn^{4+} during the perovskite film preparation process and the device work process; two extra electrons were introduced and therefore formed a heavy p-type

* Author to whom any correspondence should be addressed.

doping. Meanwhile, this oxidization process will inevitably cause the perovskite structure distortion. Secondly, during the tin perovskite film fabrication process, the nucleus formation and crystal growth rate were not balanced, which induced an unsmooth surface and pinholes in tin-based perovskite film [12–14].

The solution processing technique is widely used for tin-based perovskite layer fabrication. However, most of the solvents for the precursor solution were toxic, such as N, N-dimethyl formamide (DMF) [15–17]; and most of the anti-solvents were also toxic, such as chlorobenzene (CB) or toluene, *etc* [18, 19]. This is contrary to the intention development of environmentally friendly PSCs and hinders its commercial fabrication [20]. To avoid the use of toxic reagents, Su *et al* utilized acetic acid (HAc) as an antisolvent to regulate the perovskite film growth [21]. The crystal nucleus formation rate was accelerated and the crystal growth rate was reduced, therefore high-quality FASnI_3 perovskite film was achieved. Zhang *et al* utilized diethyl carbonate (DEC) as a green antisolvent in the FASnI_3 perovskite light absorber layers [8]. The interaction between DEC and precursor solution slowed the crystallization of perovskite, enabling a low defects film formation. Although the green antisolvent has replaced the commonly used toxic antisolvent in the above study, however, the precursor solution still contained toxic DMF. Tang *et al* used N, N-diethyl formamide (DEF) instead of toxic DMF to prepare the tin-based perovskite precursor solution [22]. DEF was slightly weaker coordinated with Sn^{2+} , rendering the formation of smaller colloids in the perovskite precursor solution, thus inducing the decreased crystal nucleus formation and retarded crystal growth, and a high-quality film was achieved.

So far, during the fabrication of a tin-based light-absorbing layer, either the precursor solution or antisolvent is toxic. Thus, it is necessary to find a green solvent strategy. In this work, we present for the first time a green-solution-proceed strategy for fabricating the tin perovskite photovoltaic cells. The $\text{FA}_{0.75}\text{MA}_{0.25}\text{SnI}_3$ precursor solution was prepared with green N, N-diethyl formamide (DEF), and 1,3-dimethyl-3,4,5,6-Tetrahydro-2(1H)-pyrimidinone (DMPU) solution; and green dibutyl ether (DEE) was used as antisolvent. In this way, perovskite films with an ideal band gap were prepared, and an efficiency of 4.4% was obtained. Moreover, the device performance remains at 80% of the initial PCE after 600 h.

2. Experimental section

2.1. Materials

Etched indium tin oxide (ITO, 7 ohm/square, Advanced); tin iodide (SnI_2 , 99.999%, Advanced); Formamidinium iodide (FAI, 99.5%, Xi'an Yuri); methylammonium iodide (MAI, 99.5%, Xi'an Yuri); C_{60} (>99%, Xi'an Yuri); Bathocuproine (BCP, >99%, Xi'an Yuri); Tin fluoride (SnF_2 , 99.9%, Macklin); 1,3-Dimethyl-3,4,5,6-tetrahydro-2(1H)-pyrimidinone (DMPU, 99%, Adamas), N, N-diethyl formamide (DEF, 99%, Adamas) and dibutyl ether (DEE,

99%, Adamas); PEDOT: PSS (4083, 1.3–1.7 wt%, Xi'an Yuri); N, N-dimethyl formamide (DMF, 99.8%, J&K); dimethyl sulfoxide (DMSO, 99.9%, J&K); chlorobenzene (CB, 99.8%, J&K); Sliver (Ag, 99.99%, Metallurgy and Materials).

2.2. Fabrication of device

2.2.1. Perovskite precursor preparation. Green solution: the $\text{FA}_{0.75}\text{MA}_{0.25}\text{SnI}_3$ perovskite precursor solution was made by MAI (27.83 mg, 0.175 mmol), FAI (90.3 mg, 0.525 mmol), SnI_2 (260.75 mg, 0.7 mmol) and SnF_2 (7.68 mg, 0.049 mmol) in 0.7 ml mixed solution of DEF and DMPU (DEF: DMPU = 6:1), and stirred overnight. The final perovskite solution concentration is 1.0 M (figures S3 and S4) and filtered by a 0.22 μm filter.

Control solution: the preparation was the same as our previous work [13]. MAI (15.9 mg, 0.1 mmol), FAI (51.6 mg, 0.3 mmol), SnI_2 (149.0 mg, 0.4 mmol), and SnF_2 (6.3 mg, 0.04 mmol) in 0.5 ml mixed solution of DMF and DMSO (DMF: DMSO = 4:1), and stirred overnight. The final perovskite solution concentration is 0.8 M and filtered by a 0.22 μm filter. The device prepared by this method is named the control device.

All these steps were carried out in a glove box (with an N_2 atmosphere).

2.2.2. Perovskite device preparation. The ITO substrates were brushed with a toothbrush dipped in the configured Hellmanex solution for at least one minute, then rinsed with plenty of deionized water, and then ultrasonic cleaned with deionized water, anhydrous ethanol, and isopropanol for every 20 min, respectively. The cleaned ITO glasses were dry with flowing nitrogen, and then UV-ozone treated for 15 min. For the fabrication of the hole transport layer (HTL), PEDOT: PSS solution was filtered by a 0.45 μm filter (PES) and spin-coated on the ozone-treated ITO glasses at 4000 rpm for 30 s, and followed with 150 $^\circ\text{C}$ anneal for 30 min. Then the ITO/PEDOT:PSS samples were immediately transferred to the nitrogen glovebox ($\text{H}_2\text{O} < 0.1$ ppm, $\text{O}_2 < 0.1$ ppm) for the following $\text{FA}_{0.75}\text{MA}_{0.25}\text{SnI}_3$ layer fabrication. 40 μl $\text{FA}_{0.75}\text{MA}_{0.25}\text{SnI}_3$ precursor solution was spin-coated at 5500 rpm for 60 s, and 130 μl DEE was dripped onto the substrates at 13 s as anti-solvent; then the substrate was annealed at 90 $^\circ\text{C}$ for 15 min (For control film: 40 μl $\text{FA}_{0.75}\text{MA}_{0.25}\text{SnI}_3$ precursor solution was spin-coated at 5000 rpm for 60 s, and 120 μl CB was dripped onto the substrates at 13 s as anti-solvent; then the substrate was annealed at 90 $^\circ\text{C}$ for 15 min). C_{60} (35 nm at 1 \AA s^{-1}), BCP (8 nm at 1 \AA s^{-1}), and Ag (80 nm) were thermal deposited on the $\text{FA}_{0.75}\text{MA}_{0.25}\text{SnI}_3$ perovskite films in a 10^{-4} Pa vacuum evaporation chamber.

2.3. Characterizations

I–V characterization: *I–V* characterization was carried out with a solar simulator (Newport AAA 1.5 G, 100 mW cm^{-2}) equipped with a Keithley 2400 in a nitrogen glovebox.

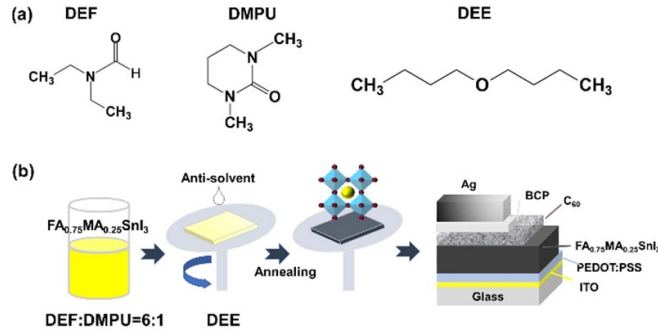


Figure 1. (a) The molecular structure diagram of DEF, DMPU, and DEE. (b) The schematic diagram of $\text{FA}_{0.75}\text{MA}_{0.25}\text{SnI}_3$ layer fabrication process.

The I - V characterization under varied light intensity (10 – 100 mW cm^{-2}) was carried out with the same setup combined with optical filters. Photoluminescence Spectroscopy (PL) was tested by a Nanolog FL3-iHR320 with 500 nm excitation wavelength. Top-view SEM was carried out with a Gemini SEM 300 at 15 kV acceleration voltage. X-ray diffraction (XRD) patterns were carried out with a D8 focus instrument from 10 to 50 degrees with 0.02 step. Contact angle measurement of perovskite films was carried out with SCI 2000 A. Ultraviolet–visible absorption spectrum (UV–Vis) measurements were performed using a UV1920 spectrophotometer from 500 – 1000 nm . Hall characterization was performed by the Hall effect tester model HL5500, and the sample structure was pure glass/perovskite film/Ag. X-ray photoelectron spectroscopy (XPS) analysis was performed using AXIS ULTRA DLD multifunctional photoelectron spectrometer with ITO/perovskite film structure. For the device stability testing, the samples were stored in the glovebox and measured I - V curves at different time points.

3. Results and discussion

The molecular structures of the green solvent DEF, DMPU, and DEE are shown in figure 1(a). Tin-based $\text{FA}_{0.75}\text{MA}_{0.25}\text{SnI}_3$ perovskite films were fabricated by one-step spin-coating method (figure 1(b)). The $\text{FA}_{0.75}\text{MA}_{0.25}\text{SnI}_3$ precursor solution was formed by dissolving perovskite with DEF and DMPU (DEF: DMPU = 6:1) solution (figure 1(b)). During the spin-coating process, green antisolvent DEE was added to the sample and followed with annealing to form $\text{FA}_{0.75}\text{MA}_{0.25}\text{SnI}_3$ film. For the comparison, we also fabricated perovskite films with DMF: DMSO = 4:1 as precursor solution and CB as anti-solvent, named as control devices in this study [13].

To explore the photophysical properties of $\text{FA}_{0.75}\text{MA}_{0.25}\text{SnI}_3$ perovskite light-absorbing layers, a series of film properties have been characterized. Firstly, XRD characterization was conducted to investigate the perovskite film crystallization (figure 2(a)). The green-solution-processed perovskite film showed similar XRD patterns with control films: the diffraction peaks were shown at 14.2° , 24.6° , 28.4° , 31.9° , and 40.6° , which corresponded to (100), (120), (200), (122) and (222)

crystal faces of the orthogonal structure of $\text{FA}_{0.75}\text{MA}_{0.25}\text{SnI}_3$ perovskite, respectively [23, 24]. Among these peaks, the diffraction peaks (100) and (200) showed a relatively high intensity, showing the preferred crystal orientation. The results show that the perovskites prepared by green solvent treatment and control group have good crystallization with a high preferred orientation in $\langle h00 \rangle$ direction. It was found that the photoluminescence spectroscopy (PL) peak value was located at 914 nm (figure 2(b)), which was also similar to that of control films. According to the Tauc Plot rule, $(ah\nu)^{1/2} = B(E_g - h\nu) = 1240/\lambda E_g = h\nu = 1240/\lambda$ (E_g was the optical band gap; a was the absorption coefficient; $h\nu$ was the photon energy and B was the constant,); the optical band gap of $\text{FA}_{0.75}\text{MA}_{0.25}\text{SnI}_3$ was calculated to be 1.32 eV , which was close to the Shockley–Queisser limit 1.34 eV [10]. Moreover, the green perovskite films showed both much higher PL intensity and absorption intensity than that of control films respectively, indicating that the film with reduced trap densities was achieved with green-solution-processed methods.

Scanning electron microscopy (SEM) was conducted to investigate the surface morphology of tin perovskite films (figures 3(a) and (b)). The control film showed polycrystalline morphology with several pinholes. In contrast, the film treated with the green solution not only has pinholes but also has blurred grain boundaries. These defects in films would trap the charge carriers and lead to serious interfacial recombination loss, therefore could result in a low short-circuit current density (J_{sc}) [25, 26]. At the same time, surface roughness was analyzed by SEM images. Figures 3(c) and (b) show the surface plot under the control condition and green condition respectively. It is found that the surface diagram under the control condition is smooth, on the contrary, the surface plot under the green condition is sharper and the film is rougher. Rough perovskite films lead to an increase in interface defects, affecting carrier transport, resulting in reduced mobility in the perovskite film (which is consistent with the Hall mobility test), and accelerating the rate of radiation recombination, resulting in lower J_{sc} [27].

To characterize the chemical changes in tin perovskite surface, the XPS Sn3d spectrum was further conducted to investigate the $\text{Sn}^{2+}/\text{Sn}^{4+}$ ratio, since Sn^{2+} to Sn^{4+} oxidation was one of the most serious issues in tin PSCs (figure 4). The peak around 487 nm (Sn $3d_{3/2}$) could be separated into two peaks

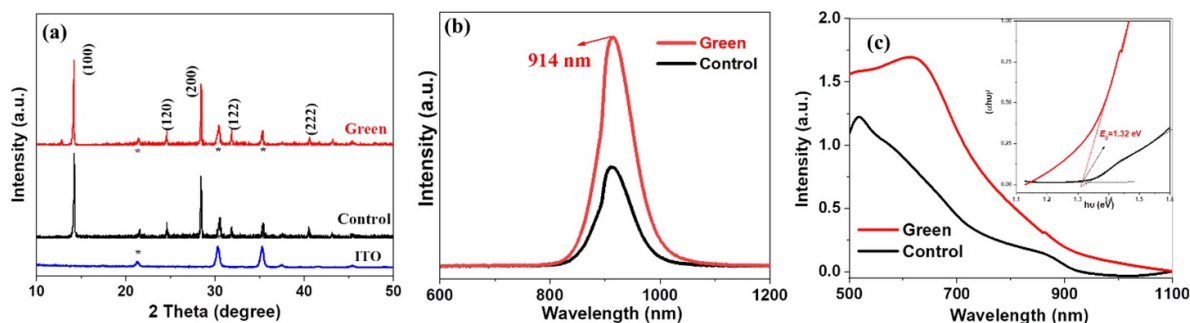


Figure 2. (a) XRD patterns, (b) steady-state photoluminescence characterization, and (c) ultraviolet–visible absorption spectrum of $\text{FA}_{0.75}\text{MA}_{0.25}\text{SnI}_3$ thin films. Note: the peaks that belonged to the ITO substrate in XRD spectra were marked as stars (*). The inset in (c) illuminates the relationship between the corresponding absorption coefficient and the photon energy.

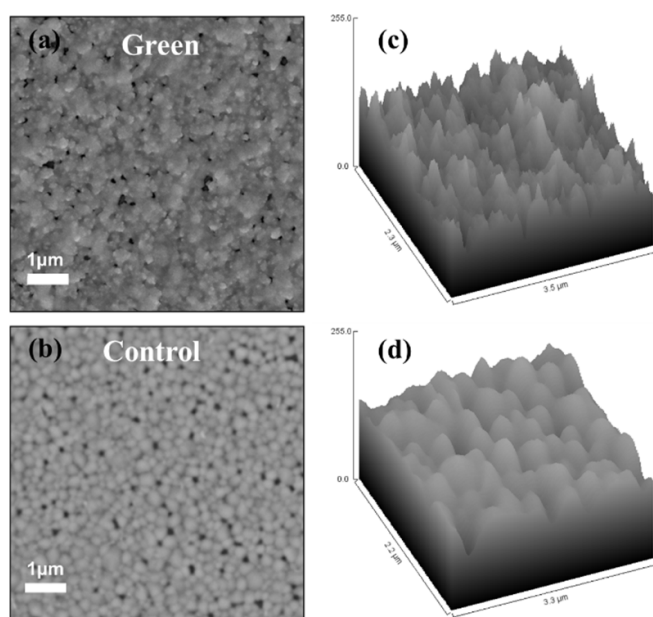


Figure 3. Top-view SEM image of (a) green-solution-processed film and (b) control film; Surface plot with the roughness of (c) green-solution-processed film and (d) control film.

at 495.1 (Sn^{2+}) and 495.7 (Sn^{4+}). The Sn^{4+} element in the green-solution-processed film was 22%, which was higher than that of the control film, which may be caused by the large pinholes in the film treated with green solution. The existence of these defects increases Sn^{2+} vacancies in the perovskite lattice, increasing Sn^{4+} content [28]. We would like to point out that for the high-performance tin PSCs, the Sn^{4+} ratio must be greatly reduced in future studies.

To further explore the hydrophobicity property of the perovskite film, the contact angle measurements were characterized (figure 5). The green-solution-processed films show a relatively hydrophobic contact angle of 62.3° , which would be beneficial for the device's stability. Moreover, we conducted Hall effect measurement to investigate the electronic properties of tin perovskite film. In the Hall effect test (figure S1), the tin-based perovskite film under green conditions showed a mobility of $92.9 \text{ cm}^{-2} \text{ V}\cdot\text{s}$ and a resistivity of 77.7 ohm cm , while the control film showed a mobility of $99.4 \text{ cm}^{-2} \text{ V}\cdot\text{s}$

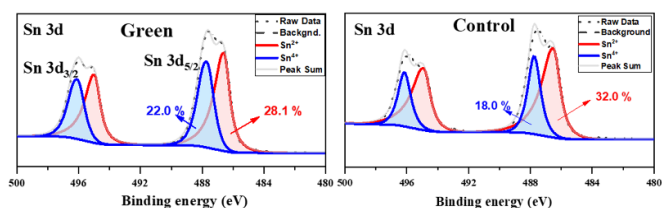


Figure 4. High-resolution XPS spectra of Sn 3d_{5/2} and 2d_{3/2}, left: green-solution-processed film and right: control films.

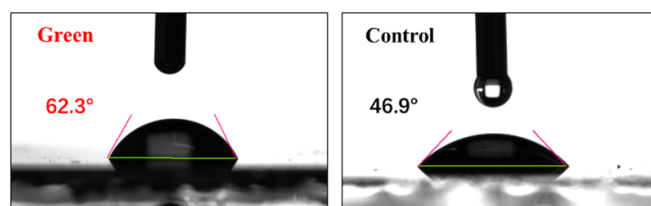


Figure 5. The water contact test of green-solution-processed perovskite film and control film.

and a resistivity of 18.5 ohm cm . Compared with the control film, the film prepared with green solution has greater resistivity and lower mobility, which may be caused by the preparation of the film is more rough, which hinders the transport of charge carriers. From the Hall effect test, compared with the control film's carrier density of $3.40 \times 10^{15} \text{ cm}^{-3}$, the carrier density of the perovskite film under green condition is $8.64 \times 10^{14} \text{ cm}^{-3}$, which is an order of magnitude smaller. The decrease in carrier density reduces the leakage current of the device and finally improves the open circuit voltage and filling factor of the device [29]. This is consistent with the results of device performance parameter testing. Meanwhile, we found that the conductive type of perovskite film prepared in green solution was n-type, while the conductive type of perovskite film in the control group was p-type, which resulted in the device prepared in green solution was not conducive to the transport of hole carriers, resulting in lower J_{sc} .

To evaluate the device performance prepared by green precursor solution and anti-solvent, a series of inverted PSCs were prepared with the structure ITO/PEDOT:PSS/ $\text{FA}_{0.75}\text{MA}_{0.25}\text{SnI}_3:\text{SnF}_2/\text{C}_{60}/\text{BCP}/\text{Ag}$;

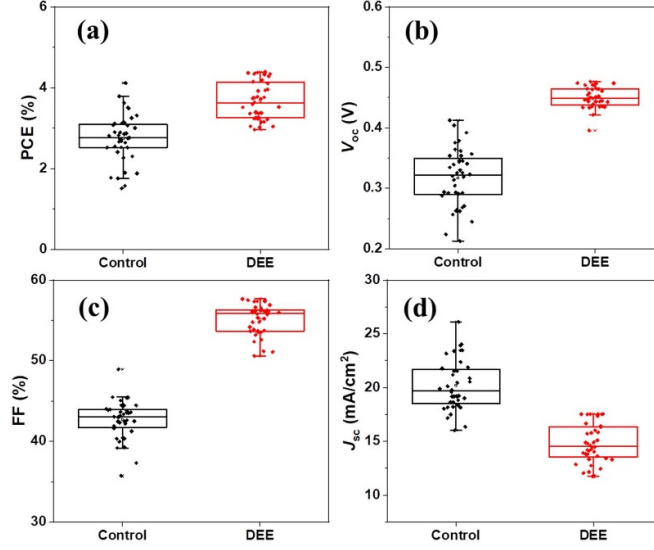


Figure 6. Statistical box chart of PSCs photoelectric performance: (a) PCE; (b) FF; (c) V_{oc} and (d) J_{sc} , respectively.

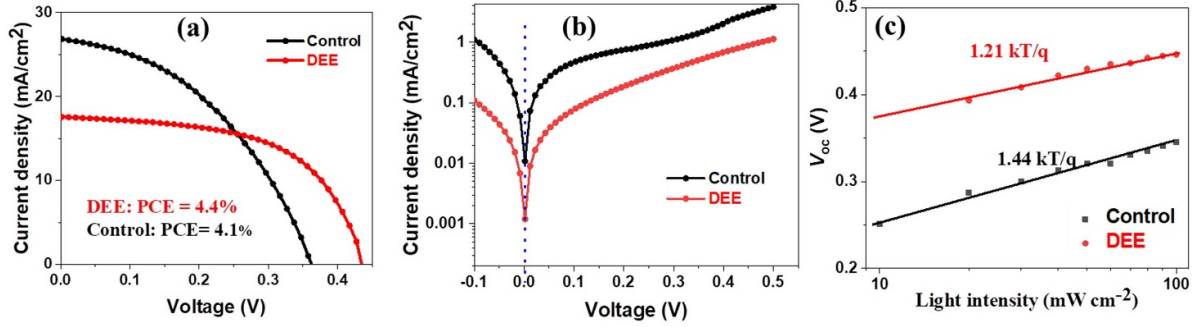


Figure 7. (a) The light J - V curves and (b) dark J - V curves of the best-performing PSCs. (c) Relationship of V_{oc} as a function of logarithmic light intensity.

where PEDOT:PSS represents poly(3,4-ethylene dioxythiophene):poly(styrene sulfonate) for HTL; and BCP represents bathocuproine for electron transport layer. The green-solution-proceed lead-free PSCs obtained a slighter higher average PCE (3.6%) than that of control, with an average FF of 54.8%, an average open circuit voltage (V_{oc}) of 0.45 V, and an average J_{sc} of 14.6 mA cm^{-2} (figure 6). The enhanced PCE was mainly attributed to the increased V_{oc} and FF; however, the J_{sc} of green-solution-proceed PSCs was much lower than that of the control device, which could be attributed to the rough surface and conductivity type of perovskite films.

For the champion green-solution-proceed device, it had achieved a PCE of 4.4%, FF of 57.4%, V_{oc} of 0.43 V, and J_{sc} of 17.6 mA cm^{-2} (figure 7(a)). Figure 7(b) shows the dark J - V curve of champion perovskite devices. By fitting the Schottky equation to the dark J - V curve, the performance parameters are analyzed by the following expression [30, 31]:

$$J = J_0 \left[\exp\left(\frac{qV}{\eta kT}\right) - 1 \right] \quad (1)$$

$$J_0 = A^* T^2 \exp\left(-\frac{q\Phi_B}{kT}\right) \quad (2)$$

Table 1. Performance parameters of PSCs by Schottky equation.

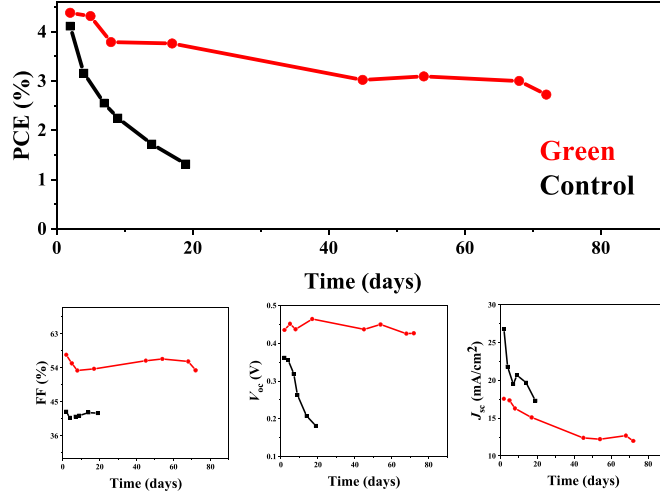
| | J_0 (mA cm^{-2}) | Φ_B (V) | η |
|---------|-------------------------------|--------------|--------|
| Green | 1.19×10^{-3} | 0.77 | 1.27 |
| Control | 1.04×10^{-2} | 0.71 | 1.39 |

where q is the electron charge, V is the voltage, k is the Boltzmann constant, T is the absolute temperature, η is the ideal factor of the diode, J_0 is the reverse saturation current density, Φ_B is the Schottky barrier height, and A^* is the Richardson's constant. The performance parameters of the PSCs obtained are shown in table 1.

Compared with the control device, the reverse saturation current density of $1.04 \times 10^{-2} \text{ mA cm}^{-2}$, the device prepared with green solution is $1.19 \times 10^{-3} \text{ mA cm}^{-2}$. The reduction of J_0 reduces the leakage current and non-radiation recombination in PSCs, which is conducive to the improvement of V_{oc} and FF. The series resistance R_s and parallel resistance R_{sh} were calculated from the light J - V curves. The actual circuit model of the photovoltaic cell is shown in figure S2. In general, the resistance of tin-based PSCs can be equivalent to the interaction of R_s and R_{sh} , where the series resistance R_s is the

Table 2. Photoelectric parameters of best-performing PSCs.

| | PCE (%) | J_{sc} (mA cm ⁻²) | V_{oc} (V) | FF (%) | R_s (Ω) | R_{sh} (Ω) |
|---------|---------|---------------------------------|--------------|--------|--------------------|-----------------------|
| Green | 4.4 | 17.6 | 0.43 | 57.4 | 63.5 | 1640.3 |
| Control | 4.1 | 26.8 | 0.36 | 42.4 | 73.5 | 525.9 |

**Figure 8.** Device performance evolution of green-solution-proceed and control PSCs: (a) PCE, (b) FF, (c) V_{oc} and (d) J_{sc} , respectively.

sum of the ohmic losses generated at the interface of positive and negative electrodes, carrier transport layer, perovskite layer, and carrier transport layer; R_{sh} was attributed to leakage paths of PSCs, such as pinholes and recombination losses in the perovskite light-absorbing layer [32, 33]. The relationship between $J-V$ characteristics of PSCs and R_s and R_{sh} was as follows [32]:

$$J_{SC} = J_{ph} - J_0 \left[\exp \left(\frac{q(V - JR_s)}{nkT} \right) - 1 \right] - \frac{JR_s}{R_{sh}} \quad (3)$$

$$V_{oc} = \left(\frac{nkT}{q} \right) \ln \left\{ \frac{J_{ph}}{J_0} \left(1 - \frac{V_{oc}}{J_{ph}R_{sh}} \right) \right\} \quad (4)$$

where J_{ph} is the photocurrent density; In an ideal situation, R_s should close to 0 and R_{sh} should close to infinity. As shown in table 2, R_s and R_{sh} of the champion device are calculated as 63.5 Ω and 1640.3 Ω , respectively, showing an improved series resistance and parallel resistance compared with that of control. Further, to explore the charge recombination dynamics in lead-free PSCs, the V_{oc} versus different light intensities were characterized, in which the relationship of V_{oc} & light intensity (Li) was shown as follows [34]:

$$V_{oc} \propto \left(\frac{nkT}{q} \right) \ln(Li) \quad (5)$$

Slope = 1 indicates that there is direct biomolecular recombination (no trap recombination), and slope = 2 means that the Shockley–Read–Hall (SRH) trap-assisted losses dominate [13, 34]. For the green-solution-proceed PSCs, it showed an improved slope of 1.21. Furthermore, it means the V_{oc} could be increased by optimized charge carrier recombination, such as

reducing the perovskite film pin-holes or improving the interfaces of perovskite/PEDOT:PSS and perovskite/ C_{60} .

With the green-solution-proceed method, the PSCs also achieved good stability. All the PSC devices were stored in a nitrogen-filled glovebox to evaluate their stability. We found that the green-solution-proceed devices still maintained 80% of the original PCE after 600 h (figure 8). In contrast, the control device was only 40% of the initial after two weeks of storage, and almost lost its photovoltaic properties.

4. Conclusions

In summary, we report for the first time, that tin-based PSCs were fabricated with a green precursor solution and a green antisolvent. Through the interaction between green solvent and antisolvent, good-quality perovskite crystal films with an ideal band gap were obtained. The electric properties were similar to that of a conventional DMF:DMSO/CB solution system. The tin-based perovskite photovoltaic devices achieved a 4.4% PCE. Moreover, the efficiency remained at 80% of the initial after 600 h of storage in a nitrogen atmosphere. This work will be helpful for the PSCs from a ‘new’ technique to an environmentally friendly ‘new and green’ technique.

Data availability statement

All data that support the findings of this study are included within the article (and any supplementary files).

Acknowledgments

This research was funded by the Natural Science Foundation of China (52002074); The Project of Construction and Support for high-level Innovative Teams of Beijing Municipal Institutions (PHR20220124); And Beijing Information Science and Technology University Program (2022PYYB12).

Conflict of interests

The authors declare no competing financial interest.

ORCID iD

Junming Li  <https://orcid.org/0000-0002-4360-7836>

References

- [1] Park J, Kim J, Yun H-S, Paik M J, Noh E, Mun H J, Kim M G, Shin T J and Seok S I 2023 Controlled growth of perovskite layers with volatile alkylammonium chlorides *Nature* **616** 724–30
- [2] Liang Z *et al* 2023 Homogenizing out-of-plane cation composition in perovskite solar cells *Nature* **624** 557–63
- [3] Snaith H J 2013 Perovskites: the emergence of a new era for low-cost, high-efficiency solar cells *J. Phys. Chem. Lett.* **4** 3623–30
- [4] Li J, Cao H-L, Jiao W-B, Wang Q, Wei M, Cantone I, Lü J and Abate A 2020 Biological impact of lead from halide perovskites reveals the risk of introducing a safe threshold *Nat. Commun.* **11** 310
- [5] Su P, Liu Y, Zhang J, Chen C, Yang B, Zhang C and Zhao X 2020 Pb-based perovskite solar cells and the underlying pollution behind clean energy: dynamic leaching of toxic substances from discarded perovskite solar cells *J. Phys. Chem. Lett.* **11** 2812–7
- [6] Chen X, Cheng J, He L, Zhao L, Zhang C, Pang A and Li J 2023 Hole transport materials for tin-based perovskite solar cells: properties, progress, prospects *Molecules* **28** 3787
- [7] Abate A 2023 Stable tin-based perovskite solar cells *ACS Energy Lett.* **8** 1896–9
- [8] Zhang Z *et al* 2023 Green-antisolvent-regulated distribution of p-type self-doping enables tin perovskite solar cells with an efficiency of over 14% *Energy Environ. Sci.* **16** 3430–40
- [9] Stoumpos C C, Malliakas C D and Kanatzidis M G 2013 Semiconducting tin and lead iodide perovskites with organic cations: phase transitions, high mobilities, and near-infrared photoluminescent properties *Inorg. Chem.* **52** 9019–38
- [10] Shockley W and Queisser H J 1961 Detailed balance limit of efficiency of p-n junction solar cells *J. Appl. Phys.* **32** 510–9
- [11] Jiang X *et al* 2021 One-step synthesis of $\text{SnI}_2 \cdot (\text{DMSO})_x$ adducts for high-performance tin perovskite solar cells *J. Am. Chem. Soc.* **143** 10970–6
- [12] Chowdhury T H, Kaneko R, Kaneko T, Sodeyama K, Lee J-J and Islam A 2022 Electronic defect passivation of FASnI_3 films by simultaneous hydrogen-bonding and chlorine co-ordination for highly efficient and stable perovskite solar cells *Chem. Eng. J.* **431** 133745
- [13] He L, Cheng J, Zhao L, Chen X, Zou X, Zhang C and Li J 2023 The defect passivation of tin halide perovskites using a cesium iodide modification *Molecules* **28** 6414
- [14] Meng X, Li Y, Qu Y, Chen H, Jiang N, Li M, Xue D-J, Hu J-S, Huang H and Yang S 2021 Crystallization kinetics modulation of FASnI_3 films with pre-nucleation clusters for efficient lead-free perovskite solar cells *Angew. Chem., Int. Ed.* **60** 3693–8
- [15] Wang M H, Wang W, Shen Y F, Cao K, Chen J, Zhao X, Xie M and Chen S 2022 Suppression of Sn^{2+} oxidation and formation of large-size crystal grains with multifunctional chloride salt for perovskite solar cell applications *J. Mater. Chem. C* **10** 10669–78
- [16] Zhu Z H, Jiang X Y, Yu D N, Yu N, Ning Z and Mi Q 2022 Smooth and compact FASnI_3 films for lead-free perovskite solar cells with over 14% efficiency *ACS Energy Lett.* **7** 2079–83
- [17] Liu X, Wang Y B, Xie F X, Yang X and Han L 2018 Improving the performance of inverted formamidinium tin iodide perovskite solar cells by reducing the energy-level mismatch *ACS Energy Lett.* **3** 1116–21
- [18] Xu L G, Zhang C, Feng X Y, Lv W, Huang Z, Lv W, Zheng C, Xing G, Huang W and Chen R 2021 Vapor incubation of FASnI_3 films for efficient and stable lead-free inverted perovskite solar cells *J. Mater. Chem. A* **9** 16943–51
- [19] Zhang Z *et al* 2022 Revealing superoxide-induced degradation in lead-free tin perovskite solar cells *Energy Environ. Sci.* **15** 5274–83
- [20] Park N-G 2021 Green solvent for perovskite solar cell production *Nat. Sustain.* **4** 192–3
- [21] Su Y, Yang J, Rao H, Zhong Y, Sheng W, Tan L and Chen Y 2023 Environmentally friendly anti-solvent engineering for high-efficiency tin-based perovskite solar cells *Energy Environ. Sci.* **16** 2177–86
- [22] Tang Z, Wang S, Zhu W, Ding L and Hao F 2023 Non-toxic solvent-processed tin-halide perovskite solar cells via weak coordination *Green Chem.* **25** 1150–6
- [23] Su Y, Yang J, Liu G L, Sheng W, Zhang J, Zhong Y, Tan L and Chen Y 2022 Acetic acid-assisted synergistic modulation of crystallization kinetics and inhibition of Sn^{2+} oxidation in tin-based perovskite solar cells *Adv. Funct. Mater.* **32** 2109631
- [24] Hao F, Stoumpos C C, Cao D H, Chang R P H and Kanatzidis M G 2014 Lead-free solid-state organic-inorganic halide perovskite solar cells *Nat. Photon.* **8** 489–94
- [25] Jiang C P, Xie Y L, Lunt R R, Hamann T W and Zhang P 2018 Elucidating the impact of thin film texture on charge transport and collection in perovskite solar cells *ACS Omega* **3** 3522–9
- [26] Saliba M, Correa-Baena J P, Grätzel M, Hagfeldt A and Abate A 2018 Perovskite solar cells: from the atomic level to film quality and device performance *Angew. Chem., Int. Ed.* **57** 2554–69
- [27] Nukunudompanich M, Budiutama G, Suzuki K, Hasegawa K and Ihara M 2020 Dominant effect of the grain size of the MAPbI_3 perovskite controlled by the surface roughness of TiO_2 on the performance of perovskite solar cells *CrystEngComm* **22** 2718–27
- [28] Wang M H, Li Y W, Zhao X Q, Riquelme A J, Anta J A, Maldivi P and Demadrille R 2022 Rational design of additive with suitable functional groups toward high-quality $\text{FA}_{0.75}\text{MA}_{0.25}\text{SnI}_3$ films and solar cells *Solar. RRL* **6** 2100800
- [29] Lee S J, Shin S S, Im J, Ahn T K, Noh J H, Jeon N J, Seok S I and Seo J 2018 Reducing carrier density in formamidinium tin perovskites and its beneficial effects on stability and efficiency of perovskite solar cells *ACS Energy Lett.* **3** 46–53

- [30] Sharma N, Negi C M S, Verma A S and Gupta S K 2018 C60 concentration influence on MEH-PPV:C60 bulk heterojunction-based Schottky devices *J. Electron. Mater.* **47** 7023–33
- [31] Singh A K and Prakash R 2012 Organic Schottky diode based on conducting polymer–nanoclay composite *RSC Adv.* **2** 5277–83
- [32] Singh R, Sandhu S and Lee J J 2019 Elucidating the effect of shunt losses on the performance of mesoporous perovskite solar cells *Sol. Energy* **193** 956–61
- [33] Tvingstedt K, Gil-Escrig L, Momblona C, Rieder P, Kiermasch D, Sessolo M, Baumann A, Bolink H J and Dyakonov V 2017 Removing leakage and surface recombination in planar perovskite solar cells *ACS Energy Lett.* **2** 424–30
- [34] Cao K *et al* 2023 Ionic compensation for defect reduction and enhanced performance of tin-based perovskite solar cells *J. Power Sources* **558** 232595